

Cycle Life Characterisation of Large Format Lithium-ion Cells

Raghavendra Arunachala¹, Kamyar Makinejad¹,
Satyajit Athlekar², Andreas Jossen², Juergen Garche³

¹TUM CREATE, Singapore, raghavendra.arunachala@tum-create.edu.sg

²Technische Universität München, Munich, Germany; ³FCBAT Ulm, Germany

Abstract

To predict the remaining useful life (RUL), commercially available lithium-ion cells of 63 Ah with nickel manganese cobalt oxide (NMC) cathode material underwent cycle life ageing tests at different current rates (C) and temperature. The key performance parameters such cell capacity, discharge capability and impedance were measured for fresh and aged cells to evaluate the RUL of the cells. The results of ageing tests showed, cell capacity was not influenced by impedance increase slightly regardless of the cycling conditions, rather power fade significant in determining the RUL of the cells. Detailed study of impedance characteristics revealed series resistance (R_{ser}) and solid electrolyte interface resistance (R_{sei}) as main contributors to power fade.

Keywords: large format cells, power fade, fast charge, remaining useful life

1 Introduction

The lithium-ion battery is characterised by superior energy density, power density, low self-discharge and long cycle life [1]. Despite these advantages, high cost, safety and ageing are the challenges to be addressed to make it a promising candidate for electric vehicle (EV) applications. Substantial research had been carried out in the past two decades to overcome these challenges [2, 3]. For EV applications the energy density is responsible for the distance range and the power density for high acceleration, high recuperation power and fast charging capability. Unfortunately, capacity fade and power fade are the main drawbacks which affect the performance of the battery over its lifetime [4]. Structural and chemical changes in the active material, electrolyte decomposition and formation of solid electrolyte interface (SEI) layer, current collector corrosion [5, 6] and separator degradation contribute to ageing [7, 8]. Recent studies show that non-uniform spatial distribution of current causes non-uniform temperature and state of charge (SOC) distribution in large format cells [9, 10]. Multi scale multidimensional modelled

by Kim et al. [11] shows the impact of the cell design on current, temperature and SOC distribution in large prismatic cells. As a result, electrical and thermal non-uniformity causes inhomogeneous ageing within the cell. Large format cells are becoming more popular in EVs due to reduced number of cells, connections and better cooling strategy for the battery pack. But limited studies have been reported on their ageing mechanisms and lifetime prediction.

In this paper we focus on accelerated ageing tests performed on large format lithium-ion cells of 63 Ah capacity to be used in a battery pack for a prototype electric taxi (E-taxi) for Singapore and evaluate its cycle life ageing characteristics. As the ageing tests using real operating conditions are time consuming and cost ineffective, accelerated ageing at high temperature and high current rate (C) were chosen to be a powerful method. The aim of this work was to study the capacity fade, power fade and fast charging capability of the cells. The cycling involving fast charging at 3C was aimed to charge the battery pack of an EV in 20 min. In a real application, repeated fast charging could be needed and sufficient cooling is required to keep the battery pack temper-

ature from exceeding 28 °C. When the battery ages due to capacity fade and power fade, the average temperature of the battery pack increases, therefore more cooling power is required to keep it from exceeding the target temperature. This paper summarises which factors influence the remaining useful life (RUL) of a battery and methods to evaluate RUL.

2 Experimental

2.1 Test matrix

Experimental studies were performed on lithium-ion high power pouch cells with the nominal capacity of 63 Ah and a nominal voltage of 3.7 V. The active material consists of graphite as anode material, $\text{LiNi}_{1/3}\text{Mn}_{1/3}\text{Co}_{1/3}\text{O}_2$ (NMC) as cathode material and LiPF_6 blended with ethylene carbonate (EC) and ethyl methyl carbonate (ECM) as electrolyte material.

Table 1: Test matrix for cycle ageing

Cell	C		Temperature °C
	Charge	Discharge	
1	1C	1C	40
2	3C	1C	25
3	1C	3C	25
4	1C	2C	25



Figure 1: Snapshot the cell tested inside Memmert TTC 256 temperature chamber

Cycle ageing tests are being performed at different temperatures and C. The test matrix is shown in Tab.1. Three cells were used in each test condition to get statistically reliable data. Thus, the total number of cells tested during this study amounts to 12.

The tests will be concluded when the cells fall below of 80% of its nominal capacity (C_N). All experiments were conducted using Digatron (MCT 200-06-6 ME S) cell testers. Each channel has

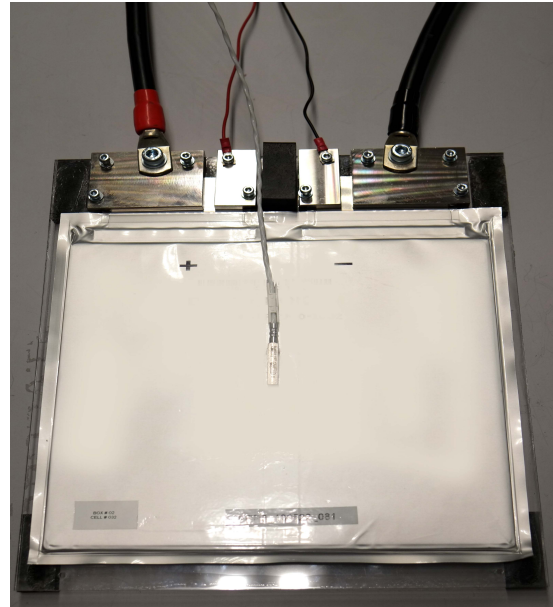


Figure 2: Cell mounted on a specially designed cell holder

the voltage range of 0 – 6 V and current range of 0.2 – 200 A. The current and voltage parameters were controlled by a linear unit CAN-LC. All experiments were conducted inside a controlled temperature environment as shown in Fig.1. The temperature chambers (Mettler TTC 256 and Espec PU-3J) were used for the purpose of maintaining high ambient conditions (40 °C) and to cool down the cells at faster rate when operating at high currents (up to 189 A). Self-made cell holders were used to mount the cells. The power and voltage sense connections were isolated. The contact screws were locked with a torque meter to provide identical surface contacts for all the cells as shown in Fig.2. The surface temperature of the cells was measured using AD 590 sensors.

2.2 Ageing and characterisation test

The cells were cycled between 2.7 V and 4.2 V. The charging was done in CCCV mode with the cut-off current 0.05C (3 A) at 4.2 V. During the discharge phase, the cells were continuously discharged to 2.7 V. Additional safety limits were used for high C cycling. If the cell temperature exceeded the safety limit during charge/discharge, it was allowed to cool down in the pause step until the temperature reduced to a safe operating condition. The safety limit for cells operating at 25 °C and 50 °C was set to 50 °C and 60 °C respectively. The tests were continued with the previous charge/discharge step. Prior to the ageing tests, initial checkup was performed on each cell by running a characterisation test at 25 °C: (1) discharge capacity, (2) hybrid pulse power characterisation (HPPC) and (3) electrochemical impedance spectroscopy (EIS). The details of these tests are described here: (1) For the discharge capacity measurement, the

cells were completely discharged to remove the residual capacity. Then they were completely charged in CCCV regime. 1 h pause time was provided between successive charge/discharge steps to attain temperature and voltage equilibrium. The fully charged cells were completely discharged at 1C to measure the cell capacity (C_1). (2) HPPC test was performed at every 10% DOD step. Prior to pulse sequence, the fully charged cells were discharged to 10% DOD at 1C and then rested for 1 h. The pulse power sequence consisted of 3C discharge for 10 s, rest at OCV for 3 min, 3C charge for 10 s and rest at OCV for 3 min [12]. After the pulse sequence, the cells were discharged by 10% DOD at 1C and rested for 1 h before starting the new pulse sequence. This procedure was repeated for every 10% DOD increment until the cells reached the cut-off voltage 2.7 V. (3) EIS characterisation was performed at every 20% DOD step starting from 0 to 100% DOD, on fully charged cells. The measurements were carried out between 700 Hz to 10 mHz at 8 points per decade and an AC amplitude of 10 mV.

After the characterisation test, the cells were cycled from a fully discharged state. To evaluate the state of health (SOH) of the cells, the ageing tests were interrupted to perform intermediate checkups after every 100 cycle step. The procedure followed during these checkups was similar to initial checkups. There was a rest period between successive characterisation and ageing tests. A rest period of 8 h and 24 h was provided to cells aged at 25 °C and 40 °C respectively. The work flow for the cycle life ageing test is shown in Fig.3.

3 Results and Discussion

3.1 Cell Capacity

At the beginning of ageing test, the capacity of each cell was measured. The average capacity for all 12 cells in the beginning was 63 ± 1.5 Ah. For this reason, normalised cell capacity was calculated for each cell by dividing by its initial value. The ageing tests were stopped periodically after every 100 cycles to monitor 1C discharge capacity of the cells at 25 °C. Fig.4 shows the normalised discharge capacity of cells tested under different cycling condition. The cells showed no capacity fade irrespective of the test conditions. Even after 400 cycles, the cell capacities were nearly constant.

Cell capacity is determined by the amount of lithium-ions available to insert into the electrode by considering the upper and lower cut-off voltage criteria. In an ideal cell all the lithium-ions should be intercalated into negative electrode at charge and back to positive electrode at discharge. But in reality not all ions are intercalated back to positive electrode as some of them are trapped and consumed to form SEI layer mainly on the anode. Hence the positive to negative electrode mass ratio designed for optimum utilization of the two electrodes is kept higher than theoretical value [13]. In the first few cycles

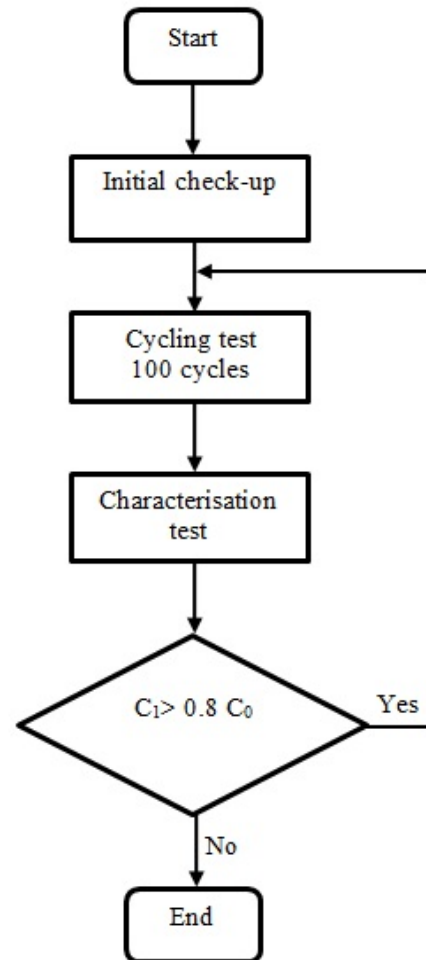


Figure 3: Flow chart for cycle life ageing test

negative electrode becomes the limitation for intercalation and at the same time formation and growth of SEI layer takes place. During this period the cell capacity is nearly equal to its initial capacity. Once the lithium-ion concentration falls below the critical value, due to trapping of more ions in the SEI layer, capacity fade will dominate the ageing [14].

3.2 Power capability

The peak power capability (PPC) of cells was evaluated by performing HPPC test as described in section 2.2 at different SOC intervals by applying a 3C current pulse for 10 seconds and measuring the voltage response. The PPC reduces as the DOD increases. For EV application, PPC at 80% and 20% interval are critical to meet both charge and discharge power demands required for the traction. The procedure to calculate PPC is explained in [15]. Figs.5a & 5b shows the normalised power capability of cells calculated from HPPC test. The cells un-

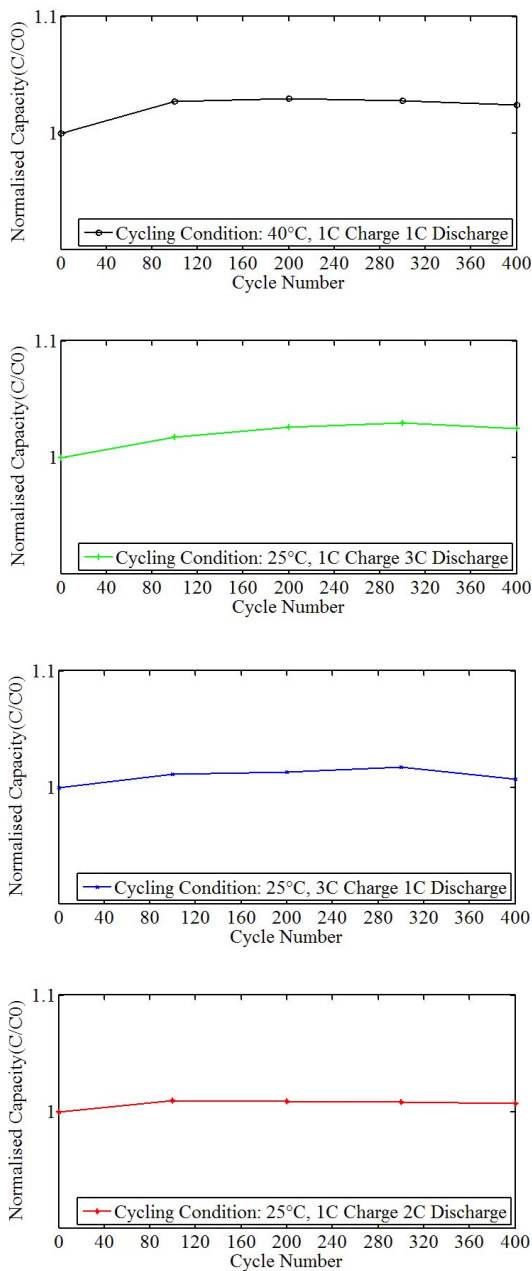


Figure 4: Normalised discharge capacity measured at 1C current, 25 °C for different cycling conditions

derwent rapid power fade in the first 100 cycles. This phenomenon occurs due to the consumption of lithium-ions during the first few cycles to form SEI layer, which increases the internal impedance of the cells. At later stages of cycling, the SEI layer continues to grow and stabilise, therefore the rate of power fade decreases with subsequent cycles. It can be also observed that power fade increased with the increase in DOD, which limited the PPC at 20% SOC. The cells cycled at 3C charge were the maximum affected. During fast charge the polarization voltage is high which causes the cells to reach the cut off voltage sooner and simultaneously tem-

perature increases rapidly due to internal heating of the cells. Since the cells were charged in CCCV, the charging mode switches to CV at 4.2 V and continues to charge until the minimum cut off current is attained. High cell voltage and high temperature increases the rate of growth of SEI layer. The cells cycled at 40 °C showed significant power fade, as high temperature increases the rate of chemical reaction leading to thicker SEI layers.

In contrast the high discharge rate showed low power fade. Impedance rise is primarily contributed by the growth of SEI layer [16]. SEI layer has linear relationship with square root of time function [17, 18]. At high discharge rates lower average voltage impeded the growth of SEI layer. The impedance rise has also resulted in steady increase in the average temperature of the cells during cycling.

This test is applicable to measure the power capability of the battery. To understand the dynamic behaviour of a battery, a more detailed frequency based EIS test is necessary. The details of this test are described in section 3.3.

3.3 Impedance spectroscopy

EIS is a common analysis method used in electrochemistry to investigate detailed cell impedance at wide range of frequencies. In this method a small sinusoidal current signal is imposed on the cell to measure its sinusoidal voltage response. The complex cell impedance at a given frequency is calculated from the input current signal and the measured voltage response by assuming the cell behaviour is linear.

The theory and measurement procedure for EIS test is described in Waag et al. [19]. The results of the EIS test are shown in Figs.6(a)–(f). In general the cell impedances were relatively higher at 20% SOC in comparison to 80% SOC under all cycling conditions. After 200 cycles there was a significant change in the impedance spectra of the cells. The series ohmic resistance (R_{ser}) increased, which is attributed to right shift in the x-intercept of impedance spectra. In the mid frequency range, a superimposition of two distinct semicircles was observed, indicating the growth of SEI layer. The mid frequency impedance is the contribution of charge transfer resistance (R_{ct}) and SEI resistance (R_{sei}) in parallel combination with the respective capacitances. Both R_{sei} and R_{ser} were dependent on SOC, which can be observed in Figs.6(b) & (e). Therefore the contribution to the power fade comes from these resistances. At 400 cycles (Figs.6(c) & (f)) R_{ser} and mid frequency section contributes to the impedance rise. The SOC dependency diminished in R_{ser} , whereas R_{sei} increased with decrease in SOC. Therefore the power capability was limited by R_{sei} . Comparison of individual cycling conditions showed that R_{sei} and R_{ser} significantly limited the power capability of the battery under 3C fast charge condition, with R_{sei} being the major contributor to ageing. At 40 °C cycling conditions, R_{sei} and R_{ser} increased at a steady rate, with R_{sei} dominating at later cycles. The high discharge

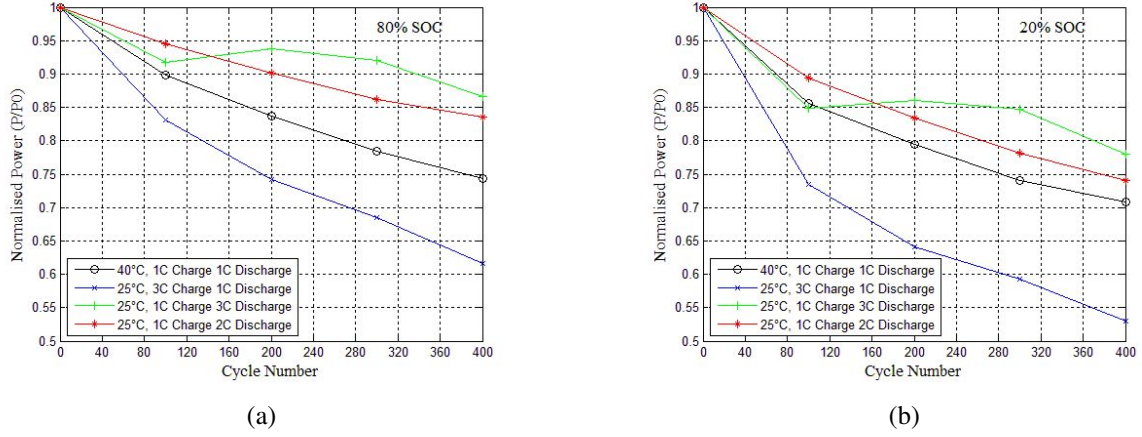


Figure 5: Normalised power capability at 25 °C for cells aged under different cycling conditions. (a) at 80% SOC (b) at 20% SOC, calculated from HPPC test

rate (3C discharge) has resulted in marginally low R_{sei} in comparison to 2C discharge. This effect was reflected in power capability comparison

3.4 Remaining useful life

Battery Management System (BMS) is an inseparable part of any EV battery, which is responsible for maintaining the battery pack within its normal operating range by predicting the battery's internal states such as State of Charge (SOC), State of Health (SOH), State of Life (SOL¹), State of Function (SOF), State of Safety (SOS), Remaining Useful life (RUL) and other internal states [20].

As these states are required by BMS to perform different tasks such as, cell balancing which is dependent on accurate SOC estimation, RUL which is dependent on accurate SOH estimation. The initial capacity of cell, also known as begin of life (BOL) capacity is an important parameter in estimating SOH. For a healthy cell, the acceptable capacity degradation range is between 0 to 20%. If the capacity of the cell falls below 80% of its BOL capacity, the end of life (EOL) of the cell is reached as described in Eq.1.

$$C_{EOL} \cong 0.8 * C_{BOL} \quad (1)$$

SOH of a cell depends on number of factors such as, number of cycles, DOD per cycle, temperature, magnitude of current, time and abuse operating conditions [21]. As shown in Eq.1, when the battery capacity reaches C_{EOL} , its SOH becomes zero.

$$SOH_C(i) = \left(1 - \frac{C_0 - C(i)}{C_0} * \frac{1}{0.2}\right) * 100 \quad (2)$$

¹SOH is used to describe the health status of the battery whereas SOL denotes the remaining life of the battery (how many cycles remain, usable charge, etc.)

C_0 is the capacity of the cell at the BOL and $C(i)$ is the capacity of the cell measured at i^{th} cycle. C_0 and $C(i)$ can be measured by cell capacity test as describe in section 3.1. Other cells parameters like impedance rise or power capability (Figs. 5 & 6) contribute to EOL as shown in Eq.3. It is important to note that when the internal impedance is twice its BOL value, EOL is reached.

$$R_{EOL} \cong 2 * R_0 \quad (3)$$

$$SOH_R(i) = \left(1 - \frac{R(i) - R_0}{R_0} * \frac{1}{0.2}\right) * 100 \quad (4)$$

R_0 refers to the discharge resistance of the cell at its BOL and $R(i)$ is the impedance of the cell measured at i^{th} cycles. R_0 and $R(i)$ can be measured by HPPC tests as described in section 3.2. RUL as a part of the BMS task informs the end user about the remaining life in the battery until its functionality is lost. In real-time application like BMS of EVs, RUL is predicted through battery model developed for the BMS, this model is based on the electrical equivalent circuit which was previously developed by authors in [22]. It is noteworthy to remember that RUL prediction is affected by multiple sources of errors like battery modelling inconsistencies, system noise and degraded sensor [23]. One method to estimate the RUL of the battery is to use the calculation of the capacity fade and the power fade as shown in Fig.7. The expression for capacity fade and power fade is described in Eqs.5 & 6.

$$pf(i) = 1 - \frac{power(i)}{power_0} = 1 - \frac{R_0}{R(i)} \quad (5)$$

$$pf(i) = 1 - \frac{capacity(i)}{capacity_0} = 1 - \frac{C_0}{C(i)} \quad (6)$$

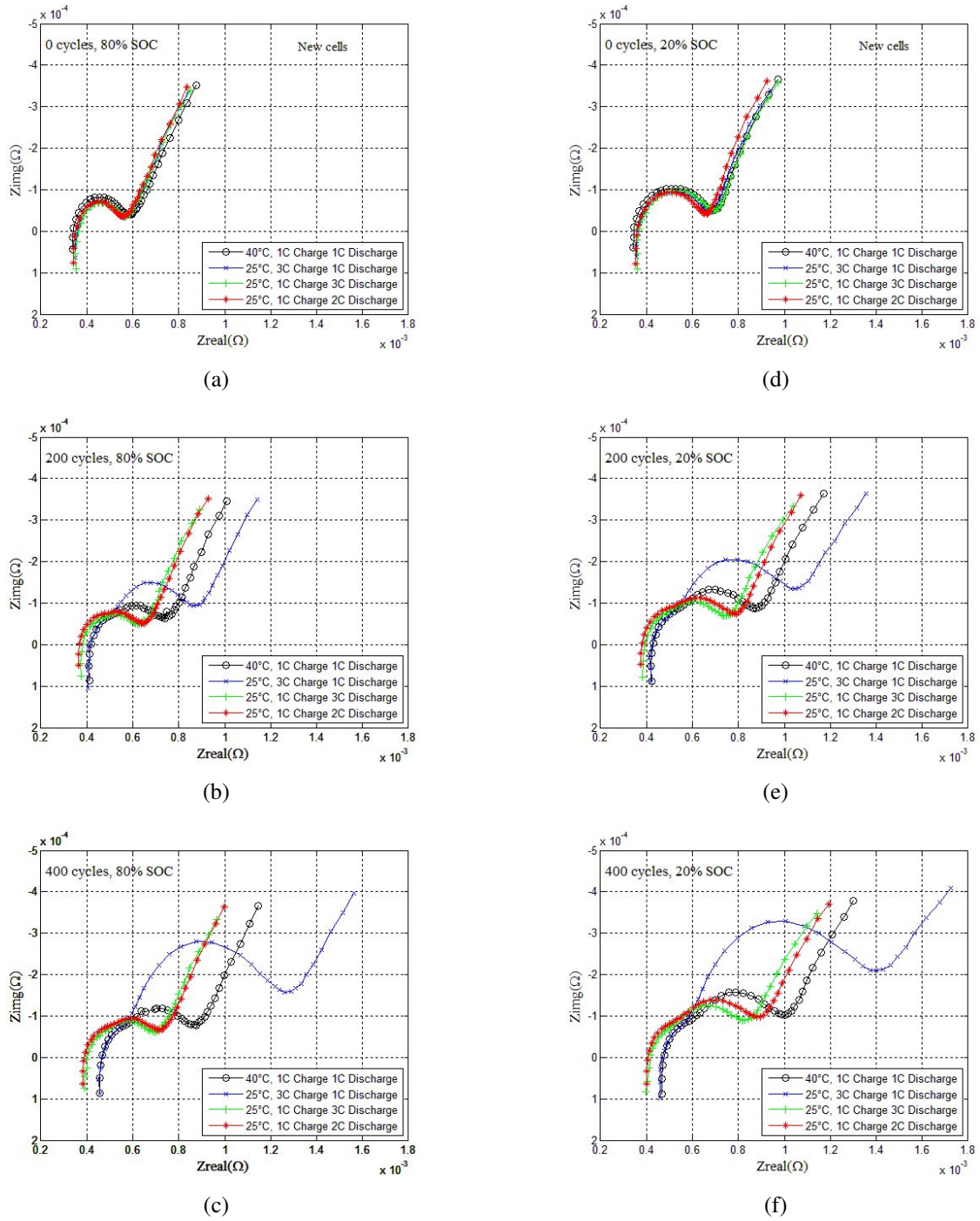


Figure 6: Nyquist plots at 25 °C for the cells aged in different cycling conditions (Fig. (a)–(c) at 80% SOC at 0, 200 and 400 cycles respectively, Fig. (d)–(f) at 20% SOC at 0, 200 and 400 cycles respectively)

The cell capacity, HPPC and EIS test results were analysed using MATLAB scripts to parameterise the cell. The reference RUL was calculated from Eq.7 as a function of power fade and capacity fade.

$$RUL(i) = f(cf(i), pf(i)) \quad (7)$$

The prediction of RUL of battery will be done in future work. The methodology to predict the

RUL is described in the flowchart in Fig.8. The particle filter algorithm and support vector machine (SVM) will be used to predict the RUL of the battery. The sensors will read the necessary output data from cell capacity, EIS and HPPC tests. Results of the cell impedance and capacitance after i cycles will be mapped based on the output of the combined algorithm. Finally the predicted RUL will be evaluated with the refer-

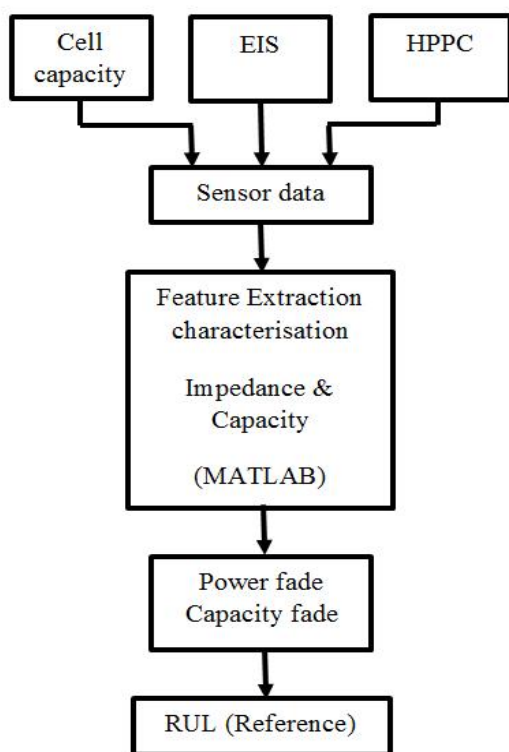


Figure 7: Flow chart of cell parameter extraction, characterisation and reference data for RUL

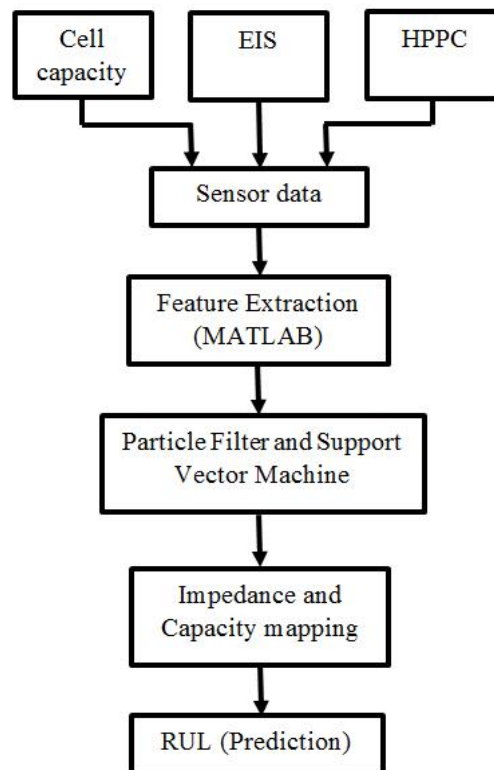


Figure 8: Flow chart of RUL prediction method

ence RUL to find the reliability of the method for EV application.

4 Conclusion

It was shown that capacities of 63 Ah cells remained nearly constant till 400 cycles under all cycling conditions (different C and temperatures). The PPC of cells reduced with the increase in number of cycles. Cells cycled under 3C fast charge and at 40 °C temperature showed significant power fade. The impedance characteristics of the aged cells showed, R_{ser} and R_{sei} resistance as dominant contributors to ageing. This work also presented the method to estimate RUL of a battery. The main findings of this work: The cell impedance has continuously increased caused by the growth of the anode SEI which leads to a decrease of the PPC, however, not of the C_1 value. The latter result contradicts with the some of the contemporary works. An explanation for our capacity result could be that only a slight increase of the R_{ser} (0.085 m Ω) till 400 cycles did not affect the C_1 discharge curve and therefore the C_1 value has not change too much. Further studies such as post-mortem analyses, conducting similar tests on short format cells of same chemistry could help the understanding of complex ageing mechanism in large format cells.

Acknowledgements

This work has been done in the framework of CREATE research programme funded by the Singapore National Research Foundation (NRF).

References

- [1] T. Dong, A. Kirchev, F. Mattera, J. Kowal, and Y. Bultel, *Dynamic modeling of Li-ion batteries using an equivalent electrical circuit*, Journal of the Electrochemical Society, ISSN 0013-4651, 158(2011), A326-A336
- [2] J. W. Fergus, *Recent developments in cathode materials for lithium ion batteries*, Journal of Power Sources, ISSN 0378-7753, 195(2010), 939-954
- [3] J. B. Goodenough and Y. Kim, *Challenges for Rechargeable Li Batteries*, *Chemistry of Materials*, ISSN 0897-4756, 22(2009), 587-603
- [4] M. Dubarry, V. Svoboda, R. Hwu, and B. Y. Liaw, *Capacity and power fading mechanism identification from a commercial cell evaluation*, Journal of Power Sources, ISSN 0378-7753, 165(2007), 566-572

- [5] J. Vetter, P. Novk, M. R. Wagner, C. Veit, K. C. Müller, J. O. Besenhard, et al., *Ageing mechanisms in lithium-ion batteries*, Journal of Power Sources, ISSN 0378-7753, 147(2005), 269-281
- [6] M. Wohlfahrt-Mehrens, C. Vogler, and J. Garche, *Aging mechanisms of lithium cathode materials*, Journal of power sources, ISSN 0378-7753, 127(2004), 58-64
- [7] C. Peabody and C. B. Arnold, *The role of mechanically induced separator creep in lithium-ion battery capacity fade*, Journal of Power Sources, ISSN 0378-7753, 196(2011), 8147-8153
- [8] X. Xiao, W. Wu, and X. Huang, *A multi-scale approach for the stress analysis of polymeric separators in a lithium-ion battery*, Journal of Power Sources, ISSN 0378-7753, 195(2010), 7649-7660
- [9] G. Zhang, C. E. Shaffer, C.-Y. Wang, and C. D. Rahn, *In-Situ Measurement of Current Distribution in a Li-Ion Cell*, Journal of The Electrochemical Society, ISSN 0013-4651, 160(2013), A610-A615
- [10] N. Martiny, P. Osswald, C. Huber, and A. Jossen, *Safety Management for Electric Vehicle Batteries in a Tropic Environment*, presented at the EVS-26, Los Angeles, California, USA, 2012
- [11] G.-H. Kim, K. Smith, K.-J. Lee, S. Santhanagopalan, and A. Pesaran, *Multi-Domain Modeling of Lithium-Ion Batteries Encompassing Multi-Physics in Varied Length Scales*, Journal of the Electrochemical Society, ISSN 0013-4651, 158(2011), A955-A969
- [12] M. Conte, F. Conte, I. Bloom, K. Morita, T. Ikeye, and J. Belt, *Ageing Testing Procedures on Lithium Batteries in an International Collaboration Context*, presented at the EVS-25, Shenzhen, China, 2010
- [13] P. Arora, R. E. White, and M. Doyle, *Capacity Fade Mechanisms and Side Reactions in Lithium Ion Batteries*, Journal of the Electrochemical Society, ISSN 0013-4651, 145(1998), 3647-3667
- [14] S. K. H. Kren, M. Cifrain, J. Garche, *The Growth of the SEI and its Influence on Capacity and Power of Li-Ion Batteries*, presented at the M3 Conference, Singapore, 16th January 2013, 2013
- [15] M. Ecker, J. B. Gerschler, J. Vogel, S. Käbitz, F. Hust, P. Dechent, et al., *Development of a lifetime prediction model for lithium-ion batteries based on extended accelerated aging test data*, Journal of Power Sources, ISSN 0378-7753, 215(2012), 248-257
- [16] A. Eddahech, O. Briat, H. Henry, J.-Y. Delétage, E. Woïrgard, and J.-M. Vinassa, *Ageing monitoring of lithium-ion cell during power cycling tests*, Microelectronics Reliability, ISSN 0026-2714, 51(2011), 1968-1971
- [17] Y. Zhang and C.-Y. Wang, *Cycle-life characterization of automotive lithium-ion batteries with LiNiO₂ cathode*, Journal of the Electrochemical Society, ISSN 0013-4651, 156(2009), A527-A535
- [18] J. Christensen and J. Newman, *A mathematical model for the lithium-ion negative electrode solid electrolyte interphase*, Journal of The Electrochemical Society, ISSN 0013-4651, 151(2004), A1977-A1988
- [19] W. Waag, S. Käbitz, and D. U. Sauer, *Experimental investigation of the lithium-ion battery impedance characteristic at various conditions and aging states and its influence on the application*, Applied Energy, ISSN 0306-2619, 102(2013), 885-897
- [20] Y. Xing, E. W. Ma, K. L. Tsui, and M. Pecht, *Battery management systems in electric and hybrid vehicles*, Energies, ISSN 1996-1073, 4(2011), 1840-1857
- [21] A. Jossen and W. Weydanz, *Moderne Akkumulatoren richtig einsetzen*, ISBN 3937536019, Ubooks, 2006
- [22] S. Thanagasundram, R. Arunachala, K. Makinejad, T. Teutsch, and A. Jossen, *A Cell Level Model for Battery Simulation*, presented at the EEVC-2012, Brussels, Belgium, 2012
- [23] B. Saha, K. Goebel, S. Poll, and J. Christophersen, *A Bayesian Framework for Remaining Useful Life Estimation*, presented at the AIAA Journal, 2007

Authors



Raghavendra Arunachala earned his B.Eng. in electrical and electronic engineering from Visveswaraya Technological University, India. He completed his M.Sc from Rheinische Westflische Technische Hochschule (RWTH) Aachen University, Germany in 2011. He is currently a doctoral student in TUM CREATE, Singapore, working in the area of electrical energy storage systems.



Juergen Garche received his PhD and habilitation (post-doctoral lecturing qualification) in theoretical and applied electrochemistry at Dresden University of Technology. He is dealing since >40 years with batteries and fuel cells. He build up the ZSW Ulm as director. Now he managed the Fuel Cell and Battery consulting office FCBAT.



Kamyar Makinejad received his B.Sc. in electrical engineering in 2007 from Shiraz University, Iran. He earned his M.Sc degree from Leibniz University of Hanover, Germany in 2011 respectively. He is currently a Research Associate in TUM CREATE in Singapore and pursuing his PhD with the Technical university of Munich. His research interest is battery diagnostic and state determination in EV applications.



Satyajit Athlekar earned his B.Eng. in mechanical engineering from Pune University, India. He is enrolled as a Masters student of Power Engineering at Technische Universität München, Germany. Currently, he is doing his master thesis at TUM CREATE, Singapore.



Andreas Jossen earned his doctorate, dealing with “Management of photo-voltaic plants using energy storage systems” at University of Stuttgart. From 1994 he was group leader for different battery related topics with ZSW, Ulm. Since 2010 he is full professor at the Institute for Electrical Energy Storage Technology, TUM.